

# DEGRADATION OF ORGANIC POLLUTANTS IN FLOCCULATED LIQUID DIGESTATE USING PHOTOCATALYTIC TITANATE NANOFIBERS: MECHANISM AND RESPONSE SURFACE OPTIMIZATION

Yiting XIAO (✉)<sup>1</sup>, Yang TIAN<sup>2</sup>, Yuanhang ZHAN<sup>1</sup>, Jun ZHU<sup>1</sup>

<sup>1</sup> Department of Biological and Agricultural Engineering, University of Arkansas, Fayetteville, AR 72701, USA.

<sup>2</sup> Material Science and Engineering Programs, University of Arkansas, Fayetteville, AR 72701, USA.

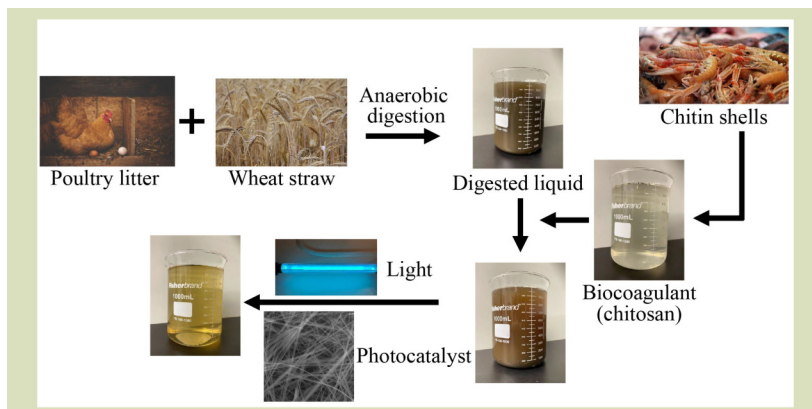
## KEYWORDS

titanate nanofibers, photocatalysis, poultry litter liquid digestate

## HIGHLIGHTS

- Titanate NFs were synthesized and photodegraded liquid digestate for the first time.
- The long titanate NFs (bandgap of 3.16 eV) have a high VFA removal rate of 72.9%.
- RSM has been used to optimize the VFA, COD, and color removal rate.
- The quadratic model and the effects of photocatalytic dosage were significant.

## GRAPHICAL ABSTRACT



## ABSTRACT

Titanate nanofibers (TNFs) were synthesized using a hydrothermal method and were employed for the first time in this study to photocatalytically degrade organic pollutants found in flocculated liquid digestate of poultry litter. The photocatalytic performance of TNFs, with a bandgap of 3.16 eV, was tested based on degradation of organic pollutants and removal of color. Five combinations of pollutant concentration and pH were examined (0.2 to 1.3 g·L<sup>-1</sup> at pH 4 to 10). Central composite design (CCD) and response surface methodology (RSM) were applied in order to optimize the removal rates of volatile fatty acids (VFA) and chemical oxygen demand (COD), and the decolorization rate. There were no significant differences between the regression models generated by the CCD/RSM and the experimental data. It was found that the optimal values for pH, dosage, VFA removal rate, COD removal rate and decolorization rate were 6.752, 0.767 g·L<sup>-1</sup>, 72.9%, 59.1% and 66.8%, respectively. These findings indicates that photocatalytic TNFs have

Received January 10, 2023;

Accepted March 31, 2023.

Correspondence: yx011@uark.edu

potential for the posttreatment of anaerobic digestion effluent, as well as other types of wastewater.

© The Author(s) 2023. Published by Higher Education Press. This is an open access article under the CC BY license (<http://creativecommons.org/licenses/by/4.0>)

## 1 INTRODUCTION

Anaerobic digestion has been widely used in industrial and municipal wastewater treatment facilities to control pollutants and recover useful energy. This creates substantial financial returns by producing methane gas and has additional benefits in reducing environmental pollution<sup>[1]</sup>. Typically, the digestate requires extensive posttreatment processes in order to meet strict discharge standards<sup>[2]</sup>. Liquid digestates are usually treated by different combinations of the following processes: struvite precipitation, advanced oxidation processes, advanced biological processes and membrane filtration<sup>[3,4]</sup>. These processes can be hazardous, leave residuals, or have high capital and recurrent costs. Additionally, valuable nutrients are rarely recovered because otherwise large quantities of digestates need to be stored, transported, and marketed according to regulatory frameworks<sup>[4]</sup>. Therefore, it is crucial to reconsider the current posttreatment techniques for anaerobic effluents to make it more sustainable.

Photocatalysts like titania (TiO<sub>2</sub>) can break down pollutants into harmless end products such as CO<sub>2</sub>, H<sub>2</sub> and mineral acids using light energy<sup>[5]</sup>. There have been extensive reports on photocatalysis in the treatment of wastewater in recent years. The majority of them, however, target synthetic wastewater of single composition or components that can be easily decomposed through the photocatalytic process, such as textile dye wastewater or paper mill wastewater. TiO<sub>2</sub> is a widely used semiconductor photocatalysis because of its chemophysical stability, low cost, and ability to completely degrade complex pollutants<sup>[6]</sup>. The titanate nanofibers (TNFs) are remarkably similar to TiO<sub>2</sub> but improved in its recyclability. These advantages of TNFs make the photocatalysis process a feasible treatment method before or after the nutrient recovery for the liquid digestate.

The objective of this study was to maximize the photodegradation efficiency of environmentally friendly TNFs on liquid digestate by optimizing its concentration and photocatalysis pH. TNFs were synthesized as one-dimensional photocatalysts to improve its recyclability through a simple hydrothermal method. Digestate from the co-digestion of poultry litter and wheat straw were selected as the substrate to assess the photocatalytic activity of TNFs in a complex

wastewater system.

## 2 MATERIALS AND METHODS

### 2.1 Digestate samples and reagents

The supernatant of the anaerobically digested poultry litter and wheat straw were obtained from an operating anaerobic sequencing batch reactor<sup>[7]</sup>. TiO<sub>2</sub> (as rutile) nanoparticles (NPs) with purity of 99.5% and a particle size ranging from 10 to 30 nm were purchased from SkySpring Nanomaterials Inc. (Houston, TX, USA) and used as is. The TNFs were synthesized in-house. The flocculant, a chitosan acetate solution, chosen in this study was purchased from Cesco Solutions Inc. (Bellingham, WA, USA). Flocculation using 5–10 mL chitosan and was conducted with 700 mL digestate without temperature adjustments. The mixtures were stirred for 10 min at 50 r·min<sup>-1</sup> and allowed to settle for 20 min. Finally, the supernatants were filtered through cheesecloth. The filtered liquid digestate was stored at 4 °C before use.

### 2.2 Synthesis of titanate nanofibers

The hydrothermal method used to prepare TNFs was a modified version of Ozkizilcik et al.<sup>[8]</sup>. Briefly, 0.875 g TiO<sub>2</sub> NPs were added to 70 mL 10 mol·L<sup>-1</sup> sodium hydroxide. The mixture was stirred continuously until it became a uniform milky suspension. Then, the suspension was transferred into a Teflon liner of a hydrothermal synthesis autoclave reactor, and the reaction was conducted at 240 °C. Finally, the white TNFs produced were collected and washed repeatedly with deionized water until the pH was close to 7.

### 2.3 Physicochemical analysis

The morphology of TNFs was observed by a scanning electron microscope (SEM) with a Philips SEM XL30 electron microscope operated at 200 kV. The crystallinity of the TNFs was analyzed by XRD on a Philips X'Pert X-ray diffractometer (Cu K $\alpha$ ,  $\lambda = 1.542 \text{ \AA}$ ) scanning from 5° to 40° (2 $\theta$ ) at a speed of 2°·min<sup>-1</sup>. The absorption spectra of the TNFs were measured using the U-0080D Diode Array Spectrophotometer (Hitachi,

Ltd., Chiyoda City, Tokyo, Japan) within the wavelength range of 190–1100 nm and the band gap energy was estimated according to the plotted graph. Chemical oxygen demand (COD) and volatile fatty acids (VFA) were measured using Hach vials (TNT 822 and TNT 872, Hach Company, Loveland, CO, USA) with a Hach DR 3900 spectrophotometer according to the manufacturer's protocol. The rate of color decomposition was measured from 190 nm to 1100 nm using Shimadzu UV-1280 spectrophotometer (Shimadzu Corporation, Kyoto, Japan) with a 10-mm quartz cuvette. The pH of the solution was determined using a PHS-25 digital-display pH meter (XL 600, Fisher Scientific, Hampton, NH, USA). The percentage reduction in COD, VFA and color of the samples were calculated as:

$$\text{COD removal} = \left(1 - \frac{C_{ci} - C_{cf}}{C_{ci}}\right) \times 100\% \quad (1)$$

$$\text{VFA removal} = \left(1 - \frac{C_{vi} - C_{vf}}{C_{vi}}\right) \times 100\% \quad (2)$$

$$\text{Color removal} = \left(1 - \frac{C_{li} - C_{lf}}{C_{li}}\right) \times 100\% \quad (3)$$

where,  $C_{ci}$  is initial COD ( $\text{mg}\cdot\text{L}^{-1}$ ),  $C_{cf}$  is final COD ( $\text{mg}\cdot\text{L}^{-1}$ ),  $C_{vi}$  is initial VFA ( $\text{mg}\cdot\text{L}^{-1}$ ),  $C_{vf}$  is final VFA ( $\text{mg}\cdot\text{L}^{-1}$ ),  $C_{li}$  is initial color (absorbance), and  $C_{lf}$  is final color (absorbance).

## 2.4 Reactor configuration design

Figure 1 illustrated the experimental arrangement for the photocatalytic reactor, which was developed for processing flocculated biogas slurry. This laboratory-scale cylinder batch

reactor was made of a 250-mm PVC pipe, with a working volume of 750 mL. The light source was composed of four low-pressure mercury lamps (11 W), which were arranged in axial alignment. The reactor was also inserted with a U-shaped glass tube for cooling to maintain the reaction temperature at around 35 °C. An electric stirrer and an air bubble stone were installed at the bottom of the reactor to ensure adequate oxidation and maintain constant agitation.

## 2.5 Experimental design

In this study, pH and concentration of TNFs were selected as independent variables to determine their effects on the photocatalytic performance of the TNFs. Each independent variable ranged over five levels between  $-\alpha$  and  $+\alpha$ , that is, 4 to 10 for pH and 0.2 to 1.3  $\text{g}\cdot\text{L}^{-1}$  for concentration. These levels were chosen based on preliminary trials of the reactor. Experimental design was conducted using the response surface methodology (RSM) through central composite design (CCD)<sup>[9,10]</sup> in the statistical software Design-Expert (version 13.0.1.0, Stat-Ease Inc, Minneapolis, MN, USA) to generate the experimental runs and determine the optimal combination of these two independent variables to maximize the three response variables, i.e., VFA removal rate, COD removal rate and decolorization rate according to the experimental results. A total of 13 ( $2^k + 2k + cp$ , where  $k$  is the number of factors and  $cp$  is the center point) experiments for the two factors with five center points were conducted. The combinations of experimental runs, and the responses obtained were presented in Table 1.

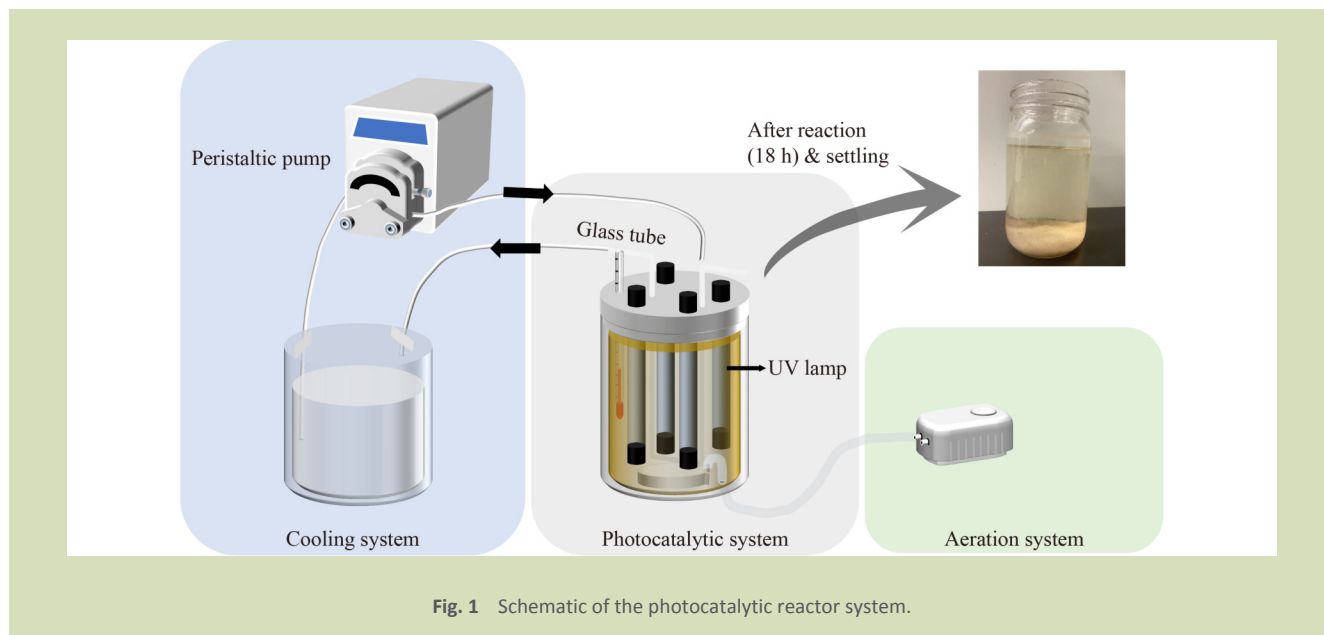


Fig. 1 Schematic of the photocatalytic reactor system.

**Table 1** Central composite design matrix of the two independent variables with experimental responses for volatile fatty acid (VFA) removal rate, chemical oxygen demand (COD) removal rate and decolorization rate

Run	pH	Concentration (mg·L <sup>-1</sup> )	VFA removal rate (%)	COD removal rate (%)	Decolorization rate (%)
1	7.00	0.75	68.0	53.2	59.9
2	7.00	1.30	51.6	10.4	18.7
3	10.0	0.75	33.1	20.7	48.1
4	9.12	0.36	30.5	18.3	54.9
5	7.00	0.75	67.4	57.8	70.8
6	4.00	0.75	38.1	37.4	42.6
7	7.00	0.75	75.6	66.3	74.3
8	4.88	1.14	57.3	39.6	42.6
9	7.00	0.20	20.9	12.8	32.8
10	4.88	0.36	47.8	38.4	49.4
11	9.12	1.14	53.1	32.3	40.2
12	7.00	0.75	74.3	59.7	60.6
13	7.00	0.75	76.4	55.7	71.1

### 3 RESULTS AND DISCUSSION

#### 3.1 Characterization of titanate nanofibers

XRD patterns of TiO<sub>2</sub> NPs and the synthesized product after the hydrothermal method were shown in Fig. 2. XRD patterns were recorded from 5° to 40° (2θ) with a step width of 0.02°. All peaks in the XRD patterns of the sodium titanate formed at different synthesis time are almost identical to each other, but the position of peaks shifted slightly. The peak shift might come from the difference of the length and diameters of the nanofibers due to change of synthesis time. The two main diffraction peaks of TiO<sub>2</sub> NPs at 25.04°, 37.6° could correspond

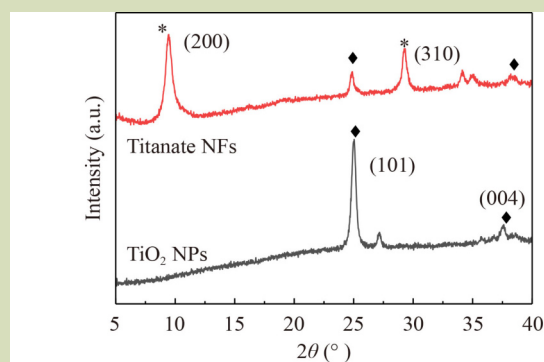


**Fig. 2** X-ray diffraction pattern for TiO<sub>2</sub> nanoparticles and Titanate nanofibers (Na<sub>2</sub>Ti<sub>2</sub>O<sub>5</sub> NFs) at different synthesis time from 1 day to 5 days (from bottom to top).

with anatase (101), (004) crystal plans, respectively (The Joint Committee on Powder Diffraction Standards (JCPDS) 83-2243), which was consistent with the manufacturer's product information. Sodium titanate nanofibers (NFs) diffraction peaks at of 2θ ~9.46° and 29.23° could be assigned to (200) and (310) plane of Na<sub>2</sub>Ti<sub>2</sub>O<sub>5</sub>·H<sub>2</sub>O (JCPDS 47-0124). The results of this study were consistent with those reported in other literature<sup>[11,12]</sup>. Based on the X-ray diffraction patterns, it can be concluded that TNFs were successfully synthesized from TiO<sub>2</sub> NPs through the hydrothermal method.

The SEM analysis of the prepared nanomaterial was done to prove the synthesis of TNFs. As shown in Fig. 3(a), the diameter of TiO<sub>2</sub> NPs was 10 to 30 nm as received, and those NPs tended to aggregate together to form a large lump. After

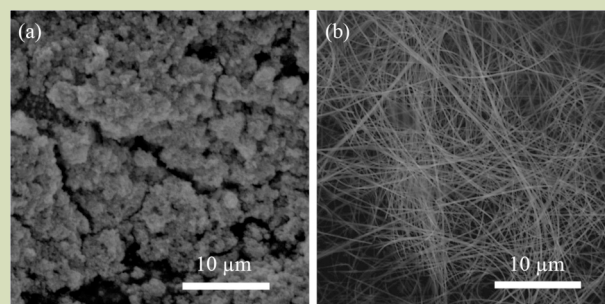


**Fig. 3** Scanning electron microscope image of (a) TiO<sub>2</sub> nanoparticles; (b) titanate (as Na<sub>2</sub>Ti<sub>2</sub>O<sub>5</sub>) nanofiber synthesized by hydrothermal method from TiO<sub>2</sub> nanoparticles.

48 h of hydrothermal treatment at 240 °C, those NPs were transformed into nanofibers with lengths ranging from tens of micrometers and width from 100 to 200 nm (Fig. 3(b)).

Current reports about the band gap of TiO<sub>2</sub> in the literature is around 3.2 eV. Energy band gap of a TNFs can be precisely calculated using the Tauc plot method<sup>[13]</sup>:

$$\alpha = \frac{A(h\nu - E_g)^n}{h\nu} \quad (4)$$

Rearranging Eq. (4) to:

$$(\alpha h\nu)^{1/n} = A^{1/n}(h\nu - E_g) \quad (5)$$

where,  $\alpha$  is the absorption coefficient,  $h = 6.626 \times 10^{-34}$  J·s, is the Planck's constant,  $\nu$  is the photon frequency, A is a proportionality constant,  $E_g$  is bandgap of the material, and  $n$  denotes the nature of the electronic transition with  $n = 2$  for direct allowed transitions. The transformed reflectance spectra plot of TNFs and the absorption spectrum is shown in Fig. 4. An estimate of the band gap energy of 3.16 eV could be obtained from the x-axis intersection point of the linear fit of the Tauc plot, which was similar but slightly smaller than that of TiO<sub>2</sub>. In other words, the synthesise of TNFs from TiO<sub>2</sub> was capable of increasing its photocatalytic activity and extending its absorption edge more toward the visible spectrum<sup>[14]</sup>.

## 3.2 Photodegradation of digestates

### 3.2.1 Effect of solution pH and concentration in preliminary experiments

Two single factor experiments were performed during the preliminary experiment to investigate the optimum operating levels of pH and concentration in terms of decolorization rate, COD and VFA removal rate. Figure S1(a) shows the effect of concentration in the range of 0.1 to 0.9, from which it could be noted that the maximum decolorization rate, COD and VFA removal rates were achieved when the concentration were at

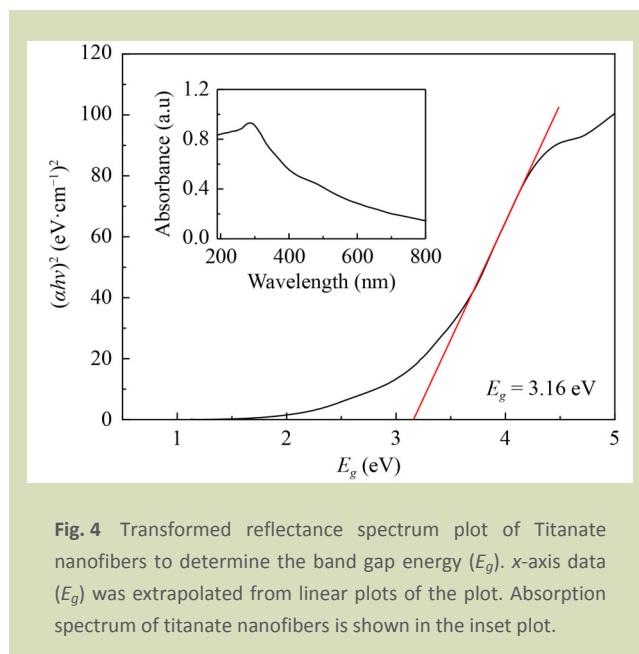


Fig. 4 Transformed reflectance spectrum plot of Titanate nanofibers to determine the band gap energy ( $E_g$ ). x-axis data ( $E_g$ ) was extrapolated from linear plots of the plot. Absorption spectrum of titanate nanofibers is shown in the inset plot.

0.7 mg·L<sup>-1</sup>. Generally, by increasing TNFs concentration, more surface area is available for adsorption of contaminants, thereby increasing degradation efficiency. However, if the concentration of TNFs continues to increase, they can block UV light or can lead to an increase in light scattering, which could decrease UV exposure and photocatalytic efficiency<sup>[15]</sup>.

Figure S1(b) illustrates the impact of pH ranging from 2.5 to 10.5 on the treatment of digestate. The highest COD removal rate and decolorization rate can be acquired at pH 2.5 and the highest VFA removal rate can be obtained at pH 6.5. These findings are inconsistent with those of Sujatha et al.<sup>[16]</sup>, who reported that the maximum COD reduction and color removal were achieved at pH 4 for degradation of coffee processing wastewater. Table 2 summarized several published articles, suggesting that different types of wastewater with varying organic pollutant levels and COD values may have different

Table 2 Comparisons with previous studies

Pollutant	Nanoparticle photocatalyst	Initial COD* (mg·L <sup>-1</sup> )	pH	Concentration (g·L <sup>-1</sup> )	UV intensity (W)	Removal efficiency (%)	Reference
Refinery wastewater	TiO <sub>2</sub> immobilized on white concrete	1200	9	0.05	24	60	[17]
Coffee processing wastewater	TiO <sub>2</sub> (addition of H <sub>2</sub> O <sub>2</sub> oxidants)	28,800	4	0.5	64	84	[16]
Refinery wastewater	TiO <sub>2</sub>	200–240	4	1.2	88	41	[18]
Metronidazole aqueous solutions	TiO <sub>2</sub>	126	10	3	125	34	[19]
Petroleum refinery wastewater	TiO <sub>2</sub>	220	4	0.1	400	83	[20]

Note: \* Indicate chemical oxygen demand.

optimal pH and concentration requirements.

Trace levels of iron were detected ( $\sim 2 \text{ mg}\cdot\text{L}^{-1}$ ) in the flocculated digestate of poultry litter. The iron (III) ions were confirmed to have the catalytic activity for oxidation of water on  $\text{TiO}_2$  by Ohno et al.<sup>[21]</sup> in that the iron (III) ions in acid solution could reduce the rate of electron-hole recombination. Consequently, in the preliminary experiments, we assume that iron ions improved the photocatalysis efficiency of the titanate nanofiber because they were involved in the Fenton process (to improve the generation rate of hydroxyl radical) to boost the degradation efficiency. This was why pH from 4 to 10 was selected in this study to ensure that Fenton process was not involved.

### 3.2.2 Quadratic model developed based on the central composite design and response surface methodology

The Design-Expert software generated three quadratic models for the two independent variables (pH and concentration) in this study using a CCD according to the experimental data in Table 1. According to the results, these models were able to fit all the three response parameters, i.e., VFA removal rate, COD removal rate, and decolorization rate fairly well. Analysis of variance (ANOVA) was also performed on the quadratic equations fitted in addition to the data fitting results to reveal

significant relationships between the independent and response variables. The regression equations using actual factors for the three response parameters were performed by Design-Expert as:

$$\begin{aligned} \text{VFA removal rate} = & 0.437429 \times \text{pH} + 1.47543 \times \text{Dosage} \\ & + 0.0398181 \times \text{pH} \times \text{Dosage} - 0.0345794 \\ & \times \text{pH}^2 - 1.00765 \times \text{Dosage}^2 - 1.39299 \end{aligned} \quad (6)$$

$$\begin{aligned} \text{COD removal rate} = & 0.30814 \times \text{pH} + 1.8034 \times \text{Dosage} \\ & + 0.038455 \times \text{pH} \times \text{Dosage} - 0.026215 \\ & \times \text{pH}^2 - 1.35626 \times \text{Dosage}^2 - 1.0786 \end{aligned} \quad (7)$$

$$\begin{aligned} \text{Decolorization rate} = & 0.279085 \times \text{pH} + 1.82114 \times \text{Dosage} \\ & - 0.0240172 \times \text{pH} \times \text{Dosage} - 0.018188 \\ & \times \text{pH}^2 - 1.19061 \times \text{Dosage}^2 - 0.95902 \end{aligned} \quad (8)$$

Table 3 presents the results of the ANOVA analysis that was used to test the significance of the developed models. With the  $F$  values ranging from 8.94 to 14.4 and the corresponding  $P$  ranging from 0.0015 to 0.006, those models were considered significant according to the goodness-of-fit tests and there was a very low chance ( $< 1\%$ ) that the  $F$  values could occur by chance. The regression model of VFA removal rate ( $F = 14.4$ ) was better than those for COD removal rate ( $F = 12.9$ ) and the decolorization rate ( $F = 8.9$ ), since the  $F$  values for the former

**Table 3** ANOVA analysis for fitting models for volatile fatty acids (VFA) and chemical oxygen demand (COD) removal rate, and Decolorization rate

ANOVA parameter	Response variable		
	VFA removal rate	COD removal rate	Decolorization rate
Sum of squares	0.378	0.390	0.274
Mean squares	0.0755	0.0780	0.0548
$R^2$	0.911	0.902	0.865
Adjusted $R^2$	0.848	0.832	0.768
Mean	0.534	0.387	0.512
Standard deviations	0.0725	0.0779	0.0783
Coefficient of variation (%)	13.6	20.17	15.3
Adequate precision	9.56	8.19	8.14
SSE*	0.0368	0.0424	0.0429
$F$	14.4	12.9	8.94
$P$	0.0015	0.0020	0.0060
(Lack of fit)			
$F$	5.24	4.36	1.94
$P$	0.0717	0.0943	0.2650

Note: \* Indicate sum of squared errors of prediction.

were larger than the latter two, respectively. In addition, the insignificant lack of fit analysis results, with the  $F$  values ranging from 1.94 to 5.24 and the corresponding  $P$  ranging from 0.0717 to 0.265 (with all  $P > 0.05$ ), indicated the adequacy of those models. Besides, the linear correlations between the observed and predicted data for the three responses were also conducted as shown in Fig. 5. The coefficients of determination ( $R^2$ ) for VFA removal rate, COD removal rate, and decolorization rate were 0.911, 0.902, and 0.865, respectively. This implied that even the model of decolorization rate with the highest  $P$  and lowest  $R^2$  still has a high correction and could explain 84.5% of the total variation. Coefficients of variation for VFA removal rate (13.6%), COD removal rate (20.1%) and decolorization rate (15.3%) indicated clear agreement between the experimental and model results. Also, all adequate precision values (measures the signal to noise ratio) for the three models were larger than 4.0, indicating signals of those models were all adequate. In conclusion, all these statistical results showed that those developed models matched the experimental data and adequately described the relationship between the variables and responses. To be more specific, these quadratic models were validated for describing VFA removal rate, COD removal rate and decolorization rate under different pH and concentration within the range used in this study.

The effect of the two variables (pH and concentration) and their interactions was presented in Table 4.  $P < 0.05$  indicated the model terms were significant. For all three models,  $\text{pH}^2$  and  $\text{concentration}^2$  are both significant model terms with very small  $P$ , which denoted their noticeable effects. However, concentration was not a significant term with regard to COD removal rate and decolorization rate. The results also demonstrated that neither the single term pH nor the interaction effect between pH and concentration were

statistically significant, meaning that the null hypothesis cannot be rejected for all those combinations. The residuals of regressions fitted using ANOVA are shown in Fig. S2. Although some terms in the model were not significant, all graphs had a random distribution of residuals, which was a characteristic of a strong regression result. Therefore, the data presented in Fig. 3 support the observation made earlier that the regression models developed could make acceptable predictions of responses to the experimental conditions used in this study.

### 3.2.3 Responses of volatile fatty acid removal rate, chemical oxygen demand removal rate, and decolorization rate to the tested variables

Surface response plots for VFA removal rate, COD removal rate and decolorization rate are shown in Fig. 6 for pH and concentration. Those plots indicate the optimal values of the response variables (VFA removal rate, COD removal rate and decolorization rate) when choosing appropriate ranges for these two variables during experimental design. For VFA removal rate, the optimal values of pH and concentration were 6.82 and 0.87  $\text{mg}\cdot\text{L}^{-1}$ , respectively, which gave the optimal removal of 73.9% (Table S1). The optimal pH and concentration for COD removal were 6.43 and 0.76  $\text{mg}\cdot\text{L}^{-1}$ , respectively, which resulted in an optimal removal of 59.4%. While decolorization rate was optimally achieved at pH 7.22 and concentration of 0.692  $\text{mg}\cdot\text{L}^{-1}$ , resulting in an optimal removal of 67.8%. Those results (Table S1) were very close to the optimal values determined by the center point of surface response plots. For the maximization of all three responses, the optimal values for pH and concentration were 6.75 and 0.77  $\text{mg}\cdot\text{L}^{-1}$ , yielding a VFA removal of 72.9%, COD removal of 59.1% and decolorization of 66.8%.

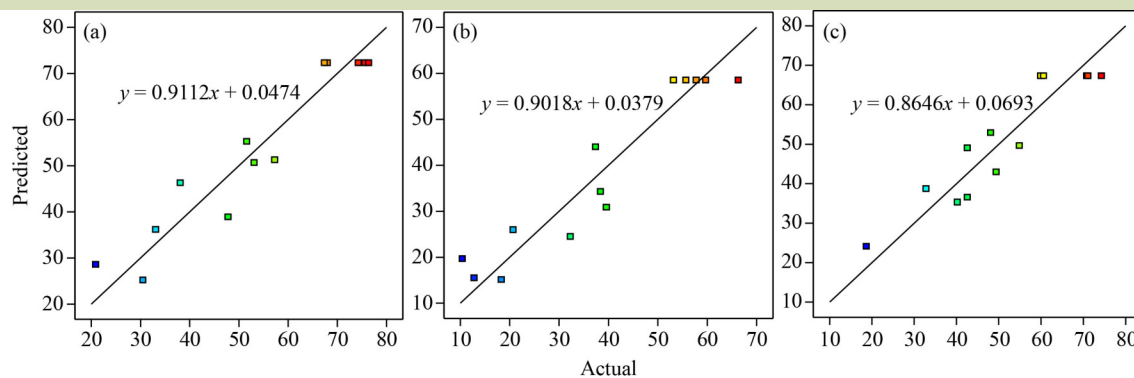
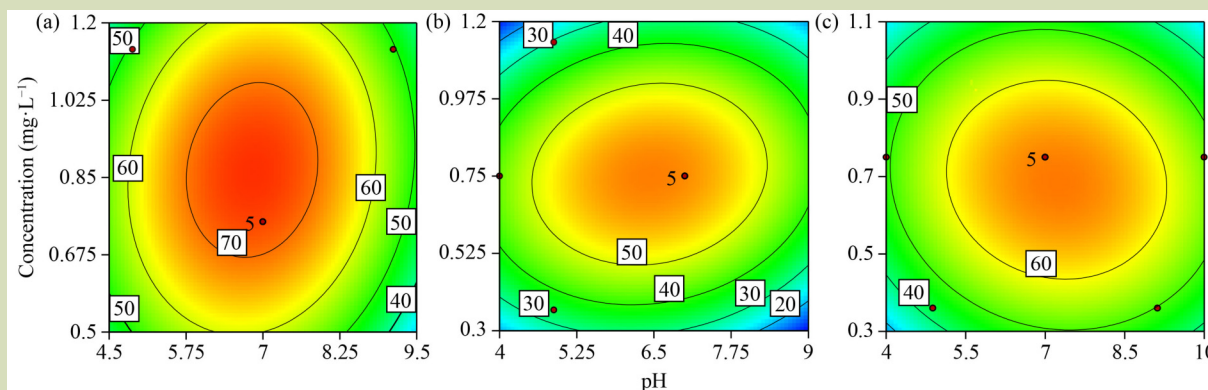


Fig. 5 Linear correlations between the observed and predicted data for volatile fatty acids (VFA) removal rate (a), chemical oxygen demand (COD) removal rate (b) and decolorization rate (c).

**Table 4** ANOVA for model variables and their interactions for volatile fatty acids (VFA) removal rate, chemical oxygen demand (COD) removal rate, and decolorization rate

ANOVA parameters	Response variables				
	pH	Concentration	pH by concentration	pH <sup>2</sup>	Concentration <sup>2</sup>
<b>VFA removal rate</b>					
Sum of squares	0.0102	0.0713	0.0043	0.168	0.162
Mean squares	0.0102	0.0713	0.0043	0.168	0.162
<i>F</i>	1.94	13.6	0.821	32.0	30.7
<i>P</i>	0.207	0.0078 <sup>a</sup>	0.395	0.0008 <sup>a</sup>	0.0009 <sup>a</sup>
<b>COD removal rate</b>					
Sum of squares	0.0325	0.0018	0.0040	0.0968	0.292
Mean squares	0.0325	0.0018	0.0040	0.0968	0.292
<i>F</i>	5.35	0.291	0.664	16.0	48.3
<i>P</i>	0.0539	0.606	0.4420	0.0052 <sup>a</sup>	0.0002 <sup>a</sup>
<b>Decolorization rate</b>					
Sum of squares	0.0015	0.0214	0.0016	0.0466	0.226
Mean squares	0.0015	0.0214	0.0016	0.0466	0.226
<i>F</i>	0.244	3.49	0.256	7.60	36.8
<i>P</i>	0.637	0.104	0.628	0.0282 <sup>a</sup>	0.0005 <sup>a</sup>

Note: <sup>a</sup> Means that the coefficients are significant.



**Fig. 6** Response surface plots of volatile fatty acid (VFA) removal rate (a) chemical oxygen demand (COD) removal rate (b), and decolorization rate (c) with respect to pH and concentration.

There is limited published reports on optimizing the COD removal rate and decolorization rate using CCD/RSM. One study by Nawaz et al.<sup>[22]</sup> reported that the highest COD removal was 78.9% when treating palm oil mill effluent through core-shell structured black TiO<sub>2</sub> (CS B-TiO<sub>2</sub>) under optimal conditions of 1.27 g·L<sup>-1</sup> CS B-TiO<sub>2</sub>, 0.06 mol·L<sup>-1</sup> H<sub>2</sub>O<sub>2</sub> (2.04 g·L<sup>-1</sup>), and pH 7.2. For comparison, the optimal values for the same parameters in this study are presented below,

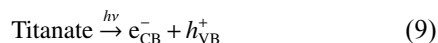
which were pH 6.75 and 0.767 mg·L<sup>-1</sup>. In their study, the photocatalysis system required a higher concentration of H<sub>2</sub>O<sub>2</sub>, which was a powerful oxidizer and could degrade organic pollutants without using photocatalysts to achieve a COD removal of 78.7%. Costa et al.<sup>[23]</sup> also reported a 79.3% color removal and 50.3% COD removal during the treatment of olive mill wastewater for a longer time of 24 h using CCD/RSM methodology.

### 3.2.4 Mechanisms

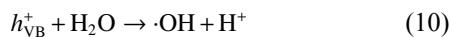
The FTIR analyses of the decomposition of flocculated digestate are shown in Fig. S3. There is a broad band with very high intensity at around  $3350\text{ cm}^{-1}$  corresponding to the vibration mode of the hydroxyl group. The major bands at around  $1635\text{ cm}^{-1}$  can be related to the C=C bond<sup>[24]</sup>, while the broad band with low intensity at around  $2160\text{ cm}^{-1}$  can be related to the C≡C bond<sup>[25]</sup>. When no photocatalysts were added into the reactor, as shown in Fig. S3(a), the IR spectra of the flocculated digestate before and after the UV treatment for 18 h were almost identical to each other. However, the intensity of these IR absorption peaks weakened or approached negligible levels if the TNFs were added into the reactor (Fig. S3(b)). The change of intensity indicated the breakdown of the aforementioned bonds, which could be attributed to the effectiveness of photocatalyst.

Figure S4 shows the mechanism of photocatalysis on an irradiated titanate particle to decompose organic pollutants. When photocatalyst particles were illuminated with light containing photons with higher energy than the bandgap of the photocatalyst, the electrons in the valence band were excited to the conduction band and formed an electron-hole pairs<sup>[26,27]</sup> (Eq. (9)). A hole ( $\text{H}^+$ ) created in valence band can oxidize  $\text{H}_2\text{O}$  molecule to hydrogen ion and hydroxyl radicals (Eq. (10)), while the excited electron can reduce oxygen gas into superoxide radical (Eq. (11)). The superoxide radical can form the uncharged hydroperoxyl radical by protonation in aqueous solution<sup>[28]</sup> (Eq. (12)) and the hydroperoxyl radical can further be decomposed into oxygen and hydrogen peroxide (Eq. (13)). Those highly reactive species are capable of participating in redox reactions with adsorbed organic pollutants on the titanate surface, resulting in their mineralization into carbon dioxide and water.

Charge carrier formation:



Oxidative species formation:



### 3.3 Feasibility analysis and research challenges

The present study explored the potential of recycling TNFs through sedimentation for the treatment of anaerobic digestates of poultry litter. Unlike other studies that employ

evaporation for recycling, this study utilizes sedimentation without incurring additional costs. However, this method can result in some remaining digestate along with residual organic matter that is attached to the surface of the TNFs. Consequently, after three cycles of recycling, the photocatalytic TNFs can experience an efficiency loss of up to 20%. However, TNFs still exhibit superior recyclability compared to  $\text{TiO}_2$  NPs due to their larger size, which facilitates easy separation from the slurry system.

Although the study has successfully synthesized TNFs and generated three significant quadratic models to describe response parameters, certain limitations exist. First, some terms in these models are not significant, which may result from the unexpected random errors and system errors, for example, the composition change during the storage of digestate in the refrigerator, the temperature variations of the control system, or the system errors of the Hach DR 3900 spectrophotometer. Second, despite TNFs having a lower bandgap than  $\text{TiO}_2$  and can be recycled easily by sedimentation, TNFs can only efficiently be activated by UV light, which carries more energy than visible light. Also, it should be noted that this study only evaluated the flocculated digestate of poultry litter, so the results obtained might not be applicable to other wastewater or even other digestate with different compositions. For example, some early studies concluded that the photocatalysis process would have a better treatment result under a lower pH, but our results indicated otherwise because a decrease for all three responses (VFA and COD removal rates and decolorization rate) was observed when pH dropped from 6.5 to 4.0. Our inference is that the high rates of COD removal and decolorization achieved at low pH in previous work were the result of the Fenton process.

## 4 CONCLUSIONS

Application of photocatalytic TNFs in treating poultry litter anaerobic digestate has shown promising results. It was found that the photocatalysis process effectively decomposed organic wastes, leading to a reduction in COD and VFA content, as well as color removal from the digestate. TNFs also demonstrated better photocatalytic efficiency than  $\text{TiO}_2$  NPs, as indicated by their slightly smaller bandgap ( $\sim 3.16\text{ eV}$ ). Using the CCD/RSM methodology, optimal running conditions for the removal of VFA, COD and color were determined to be pH 6.82 and concentration  $0.87\text{ mg}\cdot\text{L}^{-1}$ , pH 6.43 and concentration  $0.76\text{ mg}\cdot\text{L}^{-1}$ , and pH 7.22 and concentration  $0.69\text{ mg}\cdot\text{L}^{-1}$ , respectively. These conditions led to significant reductions in VFA, COD and color by 73.9%, 59.4% and 67.8%, respectively.

Overall, the use of photocatalytic TNFs for treating poultry litter digestate has proven to be an effective solution for reducing the organic waste content and removing color from

the digestate. These findings indicate that this technique could be a feasible solution for managing the liquid anaerobic digestate and/or wastewater of similar type.

### Supplementary materials

The online version of this article at <https://doi.org/10.15302/J-FASE-2023503> contains supplementary materials (Figs. S1–S4; Table S1)

### Acknowledgements

This research was supported by the Arkansas Agriculture Experiment Station of the University of Arkansas Division of Agriculture, the Center for Agricultural and Rural Sustainability, and the Graduate Professional Student Congress Tiffany Marcantonio Research Grant.

### Compliance with ethics guidelines

Yiting Xiao, Yang Tian, Yuanhang Zhan, and Jun Zhu declare that they have no conflicts of interest or financial conflicts to disclose. This article does not contain any studies with human or animal subjects performed by any of the authors.

## REFERENCES

1. Vutai V, Ma X C, Lu M. The role of anaerobic digestion in wastewater management. *EM (Pittsburgh, Pa.)*, 2016, **0**(September 2016): 12–16
2. Rongwong W, Lee J, Goh K, Karahan H E, Bae T-H. Membrane-based technologies for post-treatment of anaerobic effluents. *npj Clean Water*, 2018, **1**(1): 21
3. Monfet E, Aubry G, Ramirez A A. Nutrient removal and recovery from digestate: a review of the technology. *Biofuels*, 2018, **9**(2): 247–262
4. Selvaraj P S, Periasamy K, Suganya K, Ramadass K, Muthusamy S, Ramesh P, Bush R, Vincent S G T, Palanisami T. Novel resources recovery from anaerobic digestates: current trends and future perspectives. *Critical Reviews in Environmental Science and Technology*, 2022, **52**(11): 1915–1999
5. Frank S N, Bard A J. Heterogeneous photocatalytic oxidation of cyanide and sulfite in aqueous solutions at semiconductor powders. *Journal of Physical Chemistry*, 1977, **81**(15): 1484–1488
6. Zhang D, Dai F, Zhang P, An Z, Zhao Y, Chen L. The photodegradation of methylene blue in water with PVDF/GO/ZnO composite membrane. *Materials Science and Engineering C*, 2019, **96**: 684–692
7. Zhan Y, Cao X, Xiao Y, Wei X, Wu S, Zhu J. Start-up of co-digestion of poultry litter and wheat straw in anaerobic sequencing batch reactor by gradually increasing organic loading rate: methane production and microbial community analysis. *Bioresource Technology*, 2022, **354**: 127232
8. Ozkizilcik A, Williams R, Tian Z R, Muresanu D F, Sharma A, Sharma H S. Synthesis of biocompatible titanate nanofibers for effective delivery of neuroprotective agents. In: Skaper S D, ed. *Neurotrophic Factors: Methods and Protocols. Methods in Molecular Biology*. Vol 1727. New York: *Humana Press*, 2018, 433–442
9. Ghelich R, Jahannama M R, Abdizadeh H, Torknik F S, Vaezi M R. Central composite design (CCD)-response surface methodology (RSM) of effective electrospinning parameters on PVP-B-Hf hybrid nanofibrous composites for synthesis of HfB<sub>2</sub>-based composite nanofibers. *Composites. Part B: Engineering*, 2019, **166**: 527–541
10. Tetteh E K, Rathilal S. Response surface optimization of biophotocatalytic degradation of industrial wastewater for bioenergy recovery. *Bioengineering*, 2022, **9**(3): 95
11. Sahib S, Niu F, Sharma A, Feng L, Tian Z R, Muresanu D F, Nozari A, Sharma H S. Chapter Five—Potentiation of spinal cord conduction and neuroprotection following nanodelivery of DL-3-*n*-butylphthalide in titanium implanted nanomaterial in a focal spinal cord injury induced functional outcome, blood-spinal cord barrier breakdown and edema formation. In: Sharma H S, Sharma A, eds. *International Review of Neurobiology*. Vol 146. New Therapeutic Strategies for Brain Edema and Cell Injury. *Academic Press*, 2019, 153–188
12. Chen L, Zhou Y, Dai H, Li Z, Yu T, Liu J, Zou Z. Fiber dye-sensitized solar cells consisting of TiO<sub>2</sub> nanowires arrays on Ti thread as photoanodes through a low-cost, scalable route. *Journal of Materials Chemistry A*, 2013, **1**(38): 11790–11794
13. Makuła P, Pacia M, Macyk W. How to correctly determine the band gap energy of modified semiconductor photocatalysts based on UV-Vis spectra. *Journal of Physical Chemistry Letters*, 2018, **9**(23): 6814–6817
14. Ansari S A, Cho M H. Highly visible light responsive, narrow band gap TiO<sub>2</sub> nanoparticles modified by elemental red

- phosphorus for photocatalysis and photoelectrochemical applications. *Scientific Reports*, 2016, **6**(1): 25405
15. Chen J Q, Wang D, Zhu M X, Gao C J. Photocatalytic degradation of dimethoate using nanosized TiO<sub>2</sub> powder. *Desalination*, 2007, **207**(1–3): 87–94
  16. Sujatha G, Shanthakumar S, Chiampo F. UV light-irradiated photocatalytic degradation of coffee processing wastewater using TiO<sub>2</sub> as a catalyst. *Environments*, 2020, **7**(6): 47
  17. Gholami N, Ghasemi B, Anvaripour B, Jorfi S. Enhanced photocatalytic degradation of furfural and a real wastewater using UVC/TiO<sub>2</sub> nanoparticles immobilized on white concrete in a fixed-bed reactor. *Journal of Industrial and Engineering Chemistry*, 2018, **62**: 291–301
  18. Khan W Z, Najeeb I, Tuiyebayeva M, Makhtayeva Z. Refinery wastewater degradation with titanium dioxide, zinc oxide, and hydrogen peroxide in a photocatalytic reactor. *Process Safety and Environmental Protection*, 2015, **94**: 479–486
  19. Okhovat N, Hashemi M, Golpayegani A A. Photocatalytic decomposition of Metronidazole in aqueous solutions using titanium dioxide nanoparticles. *Journal of Materials & Environmental Sciences*, 2015, **6**(3): 792–799
  20. Shahrezaei F, Mansouri Y, Zinatizadeh A A L, Akhbari A. Process modeling and kinetic evaluation of petroleum refinery wastewater treatment in a photocatalytic reactor using TiO<sub>2</sub> nanoparticles. *Powder Technology*, 2012, **221**: 203–212
  21. Ohno T, Haga D, Fujihara K, Kaizaki K, Matsumura M. Unique effects of iron(III) ions on photocatalytic and photoelectrochemical properties of titanium dioxide. *Journal of Physical Chemistry B*, 1997, **101**(33): 6415–6419
  22. Nawaz R, Haider S, Ullah H, Akhtar M S, Khan S, Junaid M, Khan N. Optimized remediation of treated agro-industrial effluent using visible light-responsive core-shell structured black TiO<sub>2</sub> photocatalyst. *Journal of Environmental Chemical Engineering*, 2022, **10**(1): 106968
  23. Costa J C, Alves M M. Posttreatment of olive mill wastewater by immobilized TiO<sub>2</sub> photocatalysis. *Photochemistry and Photobiology*, 2013, **89**(3): 545–551
  24. Yanti, Nurhayati T, Royani I, Widayani, Khairurrijal. Synthesis and characterization of MAA-based molecularly-imprinted polymer (MIP) with D-glucose template. *Journal of Physics: Conference Series*, 2016, **739**: 012143
  25. IR Spectroscopy Tutorial: Alkynes. Available at The Organic Chemistry Lab webpage on March 10, 2023
  26. Galindo C, Jacques P, Kalt A. Photodegradation of the aminoazobenzene acid orange 52 by three advanced oxidation processes: UV/H<sub>2</sub>O<sub>2</sub>, UV/TiO<sub>2</sub> and VIS/TiO<sub>2</sub>: comparative mechanistic and kinetic investigations. *Journal of Photochemistry and Photobiology A Chemistry*, 2000, **130**(1): 35–47
  27. Marci G, Augugliaro V, López-Muñoz M J, Martín C, Palmisano L, Rives V, Schiavello M, Tilley R J D, Venezia A M. Preparation characterization and photocatalytic activity of polycrystalline ZnO/TiO<sub>2</sub> systems. 2. surface, bulk characterization, and 4-nitrophenol photodegradation in liquid–solid regime. *The Journal of Physical Chemistry B. Biophysics, Biomaterials, Liquids, and Soft Matter*, 2001, **105**(5): 1033–1040
  28. Kehler J P, Robertson J D, Smith C V. 1.14—Free Radicals and Reactive Oxygen Species. In: McQueen C A, ed. *Comprehensive Toxicology* (2nd ed). Elsevier, 2010, 277–307